Enhancement of excitonic emission in semiconductor heterostructures due to resonant coupling to multipole plasmon modes in a gold particle

A. A. Toropov, T. V. Shubina, K. G. Belyaev, S. V. Ivanov, and P. S. Kop'ev
Ioffe Physical-Technical Institute, Russian Academy of Sciences, Polytekhnicheskaya 26, 194021 St. Petersburg, Russia

Y. Ogawa and F. Minami
Department of Physics, Tokyo Institute of Technology, Meguro, Tokyo 152-8551, Japan
(Received 14 March 2011; revised manuscript received 8 June 2011; published 29 August 2011)

We apply an exact electrodynamic theory to analyze experimental data on the emission enhancement in epitaxial semiconductor structures, induced by resonant interaction of emitting excitons with plasmons localized in a gold nanoparticle. Near-field scanning optical microscopy was employed to investigate the effect of the gold particle positioned near the surface of a rough InGaN film or a CdSe/ZnSe quantum dot heterostructure fabricated by molecular-beam epitaxy. It is shown that the frequently used quasistatic approximation is unable to explain the experimental data due to the inability to take into consideration the contribution of higher-order multipole plasmon resonances. In particular, it follows from the performed calculations that the observed effect of the emission enhancement owes mainly to the resonant interaction with the quadrupole and octupole plasmon modes in the spherical gold particle. The design of optimized metal-semiconductor structures is proposed.

DOI: 10.1103/PhysRevB.84.085323 PACS number(s): 73.22.Lp, 78.67.Hc, 78.55.Cr

I. INTRODUCTION

In the recent years, there has been a revival of long-standing experimental efforts to control the spontaneous emission dynamics of a quantum emitter by the Purcell effect in metal nanostructures.[1–11] The interest is mostly stimulated by the advances in modern technology allowing fabrication of well-defined metal nanostructures supporting localized plasmons and semiconductor quantum dots (QDs) acting as single quantum emitters. In particular, it is well established at present that the rate of spontaneous recombination of the coupled "emitter-plasmon" system can be increased above that of an isolated emitter, owing to a significant local increase in the photonic mode density near the small metallic particle.

Like the Purcell effect in an optical dielectric microcavity with Bragg mirrors,[12,13] this mechanism can be useful for designing semiconductor single-photon emitting devices.[5–11] Both approaches imply resonant coupling of a QD exciton to an electromagnetic cavity mode, resulting in an increase of the emission yield and an improved light collection. These improvements can be crucial for room-temperature operation of the single-photon emitters. A potential advantage of the metal plasmonic cavity over the dielectric one is a much larger width of the resonance that simplifies achievement of the resonant conditions. The obstacle in this way is a strong dissipation of confined plasmonic modes in absorptive metals. As a result, precise optimization of the structures is an important prerequisite for substantial improvements of the radiative properties.[14] Besides, experimental implementation of the effect of the plasmonic light enhancement requires the positioning of the QD in the near optical field of the metallic particle with a nanometer-scale precision.

The plasmonic enhancement of the emission of a single quantum emitter was first detected for colloidal semiconductor nanocrystals.[5–9] A drawback of the QDs of this type for practical use is the phenomenon of blinking that is a common feature in most of them. Recently, it has been shown that the coupling of the QD to a surface plasmon weakens the blinking.[5,7] Nevertheless, the phenomenon has not been inhibited completely and these studies are currently in progress.[9] More reliable operation can be obtained in semiconductor QD structures fabricated by epitaxial techniques, molecular-beam epitaxy (MBE) or metal organic chemical vapor deposition.[15] A certain disadvantage of these structures is a relatively large density of QDs, which hampers separation of the signal from a single emitter. Recently two different approaches have been applied to achieve site-selective plasmonic enhancement of individual excitons located within a semiconductor heterostructure. An apertureless near-field scanning optical microscopy was applied to place a gold particle precisely in the vicinity of the rough surface of an InGaN film, thus amplifying and separating emission of a limited number of localized excitons emerging in the near optical field of the particle.[10] The other technique implies fabrication of hybrid metal-semiconductor structures containing mutually ordered arrays of InGaAs QDs and indium nanocrystals.[11] Both investigations qualitatively confirm applicability of the concept of plasmonic enhancement to the emission of single excitons in epitaxial nanostructures. Nevetheless, no quantitative theoretical analysis of these results has been so far presented.

The objective of this paper is to apply an exact electrodynamic theory in order to analyze and interpret the experimental results on the plasmon-induced enhancement of the excitonic emission in InGaN films and self-organized CdSe/ZnSe QDs fabricated by MBE. The effect is achieved due to the resonant interaction of the localized excitons with plasmons confined in a gold nanoparticle, whose precise positioning is performed by means of a near-field scanning optical microscope (NSOM). We show that the frequently used semiclassical theory[16–18] fails to explain the data even qualitatively due to the inability to take into account the contribution of higher-order plasmonic modes. Furthermore, we analyze the behavior of the amplification factor of emission versus various parameters and propose the design of optimized metal-semiconductor structures.

The paper is organized as follows. In Sec. II we formulate the theory, provide the results of numerical calculations, demonstrate the role of different parameters of the coupled exciton-plasmon system, and propose the examples of optimized structures. Section III describes the experimental results and provides their theoretical interpretation. Section IV summarizes and concludes the paper.

II. ELECTRODYNAMIC CALCULATIONS

Previously many authors considered properties of the emitters interacting with metal nanostructures in a quasistatic model.[16–19] This approximation, however, is applicable only to small enough metal particles and neglects some important effects, like, e.g., phase retardation and coupling of the radiation to higher-order plasmon modes in the metal particle.[14] A distinctive feature of the metal-semiconductor structures is a relatively large permittivity of the semiconductor medium, surrounding the metallic particle. For example, in GaAs and InAs the permittivity is as large as 13–14. Therefore the wavelength of light in semiconductors, corresponding to the plasma resonance, can be as short as ~100 nm, and the plasmon properties of the particles of a comparable size should be considered in the framework of the exact electrodynamic theory.

The electromagnetic interaction of an emitting exciton with a metal nanoparticle is strongly dependent on their dielectric environment. For the described NSOM experiments, the permittivity of the surrounding medium ε_m fluctuates on a microscopic level due to the complicated relief of the semiconductor surface. It can hardly be determined with a reasonable accuracy for any accidental position of the NSOM tip in the vicinity of the semiconductor structure. As a reasonable approximation, the fluctuating dielectric surrounding can be substituted by a homogeneous medium with an effective ε_m.[20] Then the value of ε_m is dependent on the tip position, varying between the ambient permittivity and the permittivity of the semiconductor.

We have used an exact electrodynamic theory formulated for a dipole emitter and a metal sphere (of radius a) embedded in a homogeneous nonabsorbing dielectric medium with permittivity ε_m and located at a distance d from each other.[21–24] Within this formalism, the decay rates of the emitter are calculated analytically in terms of expansions in ordinary spherical functions for both the radial and tangential orientations of the dipole with respect to the surface of the sphere. For the radial orientation, the total decay rate ($\gamma_\perp$) and the radiative decay rate ($\gamma_\perp^R$) of the emitter can be expressed as

$$\frac{\gamma_\perp}{\gamma_0} = 1 + \frac{3}{2}\mathrm{Re}\sum_{n=1}^{\infty} n(n+1)(2n+1)B_n\left[\frac{h_n^{(1)}(k_m r)}{k_m r}\right]^2 \quad (1)$$

and

$$\frac{\gamma_\perp^R}{\gamma_0} = \frac{3}{2}\sum_{n=1}^{\infty} n(n+1)(2n+1)\left|\frac{j_n(k_m r) + B_n h_n^{(1)}(k_m r)}{k_m r}\right|^2, \quad (2)$$

where γ_0 is the radiative decay rate in the absence of the metal sphere, $r = a + d$, $k_m = \sqrt{\varepsilon_m}\omega/c$, ω is the frequency of the emission, c is the speed of light in vacuum, n is the angular mode number, $h_n^{(1)}$ and j_n are the ordinary spherical Hankel and Bessel functions. A_n and B_n are the Mie scattering coefficients defined as

$$A_n = \frac{j_n(k_m a)\psi_n'(ka) - j_n(ka)\psi_n'(k_m a)}{j_n(ka)\xi_n'(k_m a) - h_n^{(1)}(k_m a)\psi_n'(ka)}, \quad (3)$$

$$B_n = \frac{\varepsilon_m j_n(k_m a)\psi_n'(ka) - \varepsilon j_n(ka)\psi_n'(k_m a)}{\varepsilon j_n(ka)\xi_n'(k_m a) - \varepsilon_m h_n^{(1)}(k_m a)\psi_n'(ka)}, \quad (4)$$

where $\psi_n(x) \equiv x j_n(x)$, $\xi_n(x) \equiv x h_n^{(1)}(x)$, $k = \sqrt{\varepsilon}\omega/c$, and ε is the complex permittivity of the metal.

The corresponding decay rates for the tangential orientation ($\gamma_\parallel$ and $\gamma_\parallel^R$) are given by

$$\frac{\gamma_\parallel}{\gamma_0} = 1 + \frac{3}{2}\mathrm{Re}\sum_{n=1}^{\infty}\left(n+\frac{1}{2}\right) \times\left(B_n\left[\frac{\xi_n'(k_m r)}{k_m r}\right]^2 + A_n\left[h_n^{(1)}(k_m r)\right]^2\right), \quad (5)$$

and

$$\frac{\gamma_\parallel^R}{\gamma_0} = \frac{3}{4}\sum_{n=1}^{\infty}(2n+1)\left[\left|j_n(k_m r) + A_n h_n^{(1)}(k_m r)\right|^2 + \left|\frac{\psi_{n'}(k_m r) + B_n\xi_{n'}(k_m r)}{k_m r}\right|^2\right]. \quad (6)$$

Both $\gamma_\perp$ and $\gamma_\parallel$ refer to the decay of the emitter with the 100% emission yield in the absence of the metal sphere. Equations similar to Eqs. (1)–(6) were derived by Kim *et al.*[24] for an interacting dipole emitter and a metal particle placed in vacuum. To apply the formulas presented there for the case of the emitter and the particle located in the medium with a permittivity ε_m we have replaced in Eqs. (1)–(6) the metal permittivity ε by $\varepsilon/\varepsilon_m$ and redefined $k_m = \omega/c$ as $k_m = \sqrt{\varepsilon_m}\omega/c$.

The emission yield of the emitter with the nonzero nonradiative decay in the absence of the metal sphere can be derived as

$$Y_i = \frac{\gamma_i^R}{\gamma_i + \Gamma_0^{NR}} = \frac{\gamma_i^R/\gamma_0}{\gamma_i/\gamma_0 + \frac{1-Y_0}{Y_0}}, \quad (7)$$

where $Y_0 = \Gamma_0^R/(\Gamma_0^R + \Gamma_0^{NR})$, Γ_0^R and Γ_0^{NR} are the radiative and nonradiative decay rates of the isolated emitter, and index i defines either $\perp$ or $\parallel$. Deriving Eq. (7) we assume that $\Gamma_0^R = \gamma_0$. Equations (1)–(7) allow one to calculate the emission enhancement factor $K_{em} = Y/Y_0$ as a function of different parameters. The number of angular modes required for reasonable convergence of the infinite summations in Eqs. (1), (2), (5), and (6) depends on the distance between the emitting dipole and the surface of the gold particle. Only lowest resonant modes should be taken into account if the distance is large enough (more than ~20 nm). The higher-order nonresonant plasmon modes are significant at very small distances. Interaction with these modes always reduces the emission yield since they do not couple to the far field.[14]

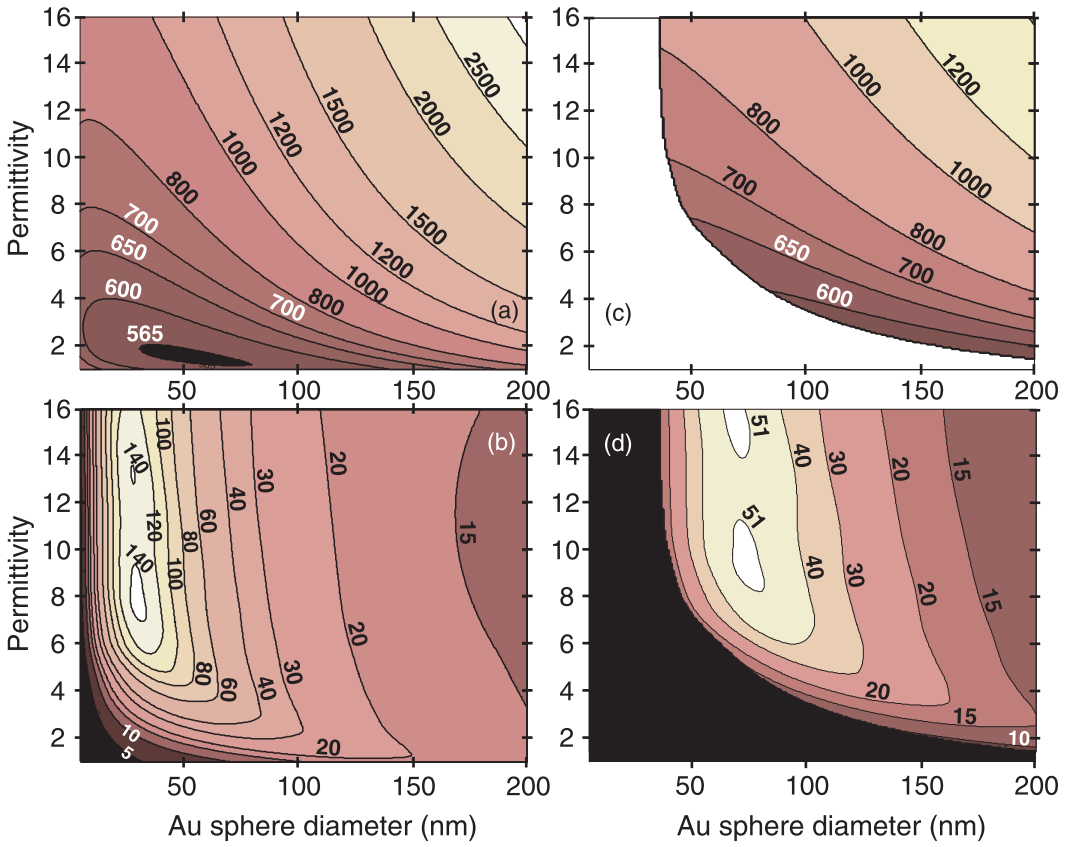

FIG. 1. (Color online) Two-dimensional contour plots of the resonance wavelength (a), (c) and respective light amplification factor (b), (d), calculated for the dipole (a), (b) and quadrupole (c), (d) plasmon resonances as a function of the diameter of the gold sphere and the effective permittivity. The calculation is performed for the radial orientation of the emitting dipole with respect to the surface of the sphere. The distance between the sphere and the emitter is 4 nm and the initial emission yield of the emitter is $Y_0 = 0.001$.

Note that for the distance smaller than ∼1 nm the considered purely electrodynamic model is not valid since under these conditions electronic energy transfer between the emitter and metal should be taken into account. To obtain reasonable convergence down to this limiting separation the summation in Eqs. (1), (2), (5), and (6) should be carried out over ∼50 angular modes.

There are many factors that determine emission properties of the system "QD-metal particle." The shape and size of the particle, as well as dielectric functions of the metal and the surrounding dielectric medium, control the position, strength, and spectral width of the plasmon-induced resonances in the spectrum of the emission enhancement factor. In the presented calculations we fix the spherical shape of the metal particle as well as the dielectric function of gold, as taken from Ref. 25. The diameter of the metal sphere and the effective permittivity are considered as varying parameters. Gold is chosen as a promising plasmonic metal due to a relatively small imaginary part of its dielectric function in visible and near-IR spectral ranges, as wells as due to high chemical stability. The gold particle with a spherical shape can be readily obtained, e.g., by precipitation from a colloidal solution.

Another important parameter is the distance d between the emitter and the surface of the metal sphere. There is an optimum value of $d \simeq 4$–15 nm, since the emitter-plasmon interaction is rapidly weakened at larger d, while at the smallest distances the enhancement factor decreases due to efficient coupling of the radiation to the dissipative higher-order plasmonic modes of the metallic particle.[14] The efficiency of the enhancement also drastically depends on the initial emission yield of the emitter in the absence of the metal particle (Y_0). The smaller is Y_0, the larger is the enhancement factor. It follows readily from Eq. (7) that for the value $Y_0 = 1$, K_{em} is less than 1, since γ_i is always larger than γ_i^R, being the sum of γ_i^R and the rate of the nonradiative decay governed by dissipative losses in the metal. Finally, the enhancement factor strongly depends on the dipole polarization with respect to the surface of the metal particle. The enhancement is much stronger for the dipole oriented normally to the surface of the metal particle (radial orientation) as compared to the tangential orientation. This phenomenon owes to the constructive (radial orientation) and destructive (tangential orientation) interference of the source and image dipoles. At the frequency of the plasmonic dipole resonance the ratio of the enhancement factors for the two orientations can be about one order of magnitude.[14,16]

Using Eqs. (1)–(7) we calculate the emission enhancement factor at the wavelengths of different plasmonic resonances as a function of the diameter of the gold sphere and the effective permittivity of the semiconductor medium. The distance between the dipole and the sphere was fixed at the value corresponding to the maximum enhancement. Two-dimensional contour plots in Fig. 1 show the representative data obtained

for the radial orientation of the emitting dipole both for the dipole [Figs. 1(a) and 1(b)] and quadrupole [Figs. 1(c) and 1(d)] plasmon resonances. For the demonstrative purpose we fix a rather small value 0.1% of the emission yield of the emitter in the absence of the metal sphere. The variation of the diameter of the sphere between 5 and 200 nm and ε_m in the range 1–14 allows one to modify the wavelength of the dipole resonance between 560 and 2800 nm [Fig. 1(a)] and the wavelength of the quadrupole resonance between 590 and 1300 nm [Fig. 1(c)]. Note that the dipole mode contributes to the plasmonic enhancement in the whole space of the parameters, whereas the contribution of the higher-order multipole modes exists only for large enough metal particles and effective permittivity ε_m.

For the dipole resonance the enhancement is most efficient for the sphere diameter in the range $10 < 2a < 70$ nm and $\varepsilon_m > 4$. For the higher-order modes the optimal range is shifted toward larger sizes of the metal particle. For all resonances the maximum enhancement corresponds to the spectral range 700–900 nm, where the imaginary part of the dielectric function of gold has lowest values.[25] The maximum value of K_{em} achieved at the wavelength of the quadrupole-mode resonance [Figs. 1(c) and 1(d)] and of other higher-order resonances is typically 2–3 times smaller than for the dipole-mode resonance at the same wavelength. For the dipole mode, the maximum possible value of K_{em} is ~140 for $Y_0 = 0.001$ (0.1%), ~35 for $Y_0 = 0.01$ (1%), ~10 for $Y_0 = 0.05$ (5%), ~5 for $Y_0 = 0.1$ (10%), and ~1 for $Y_0 = 0.5$ (50%).

These data define the semiconductor structures most promising for implementation of the effect of plasmonic enhancement employing gold spherical particles. They should emit light in the range 700–900 nm provided the effective permittivity and the size of the particle are within the range of optimal values. For example, the amplifying emitter can be an exciton localized within a self-organized QD fabricated in the system of III–V semiconductor compounds (In,Al,Ga)As possessing permittivity ~13–14. The emission wavelength in these structures can be tuned flexibly between 650 and 1100 nm.[26,27] Then, one can conclude from Figs. 1(a) and 1(b) that the maximum possible efficiency of the enhancement can be achieved with the gold particle 30–40 nm in diameter, which is either completely or partly embedded into the semiconductor medium. Note that, to the best of our knowledge, the emission enhancement in III–V self-organized QDs due to interaction with plasmons in gold nanostructures has never been observed experimentally.

Of particular interest are the structures emitting at the telecommunication wavelengths 1.3 and 1.55 μm. Using rather large gold particles (100–150 nm in diameter) embedded in the semiconductor with the effective permittivity in the range 6–14, it is possible to achieve at these wavelengths the enhancement factor as large as ~15–25 for $Y_0 = 0.001$ [see Figs. 1(a) and 1(b)], ~10–15 for $Y_0 = 0.01$, ~4–5 for $Y_0 = 0.05$, and ~2.5–3 for $Y_0 = 0.1$.

III. EXPERIMENTAL RESULTS AND DISCUSSION

The samples chosen for the experimental studies of the effect of plasmonic enhancement are an $In_{0.25}Ga_{0.75}N$ film and a CdSe/ZnSe QD heterostructure, fabricated by MBE. A 200-nm-thick layer of InGaN was deposited by plasma-assisted MBE above a GaN buffer layer grown on a *c*-oriented sapphire substrate. The sample was grown under N-rich conditions to provide a nanocolumnar film morphology with the surface roughness on the scale of 100 nm.[28] The effect of site-selective enhancement of emission was previously observed in this sample by means of apertureless NSOM.[10] In the CdSe/ZnSe heterostructure the ZnCdSe QDs are self-organized within a 2.5-monolayer-thick CdSe layer buried within a ZnSe matrix 10 nm below the surface.[29] The morphology of the structure is generally flat besides the sites where extended defects meet the surface, disturbing the surface flatness.[30] Strong localization of excitons occurs in the structures of both types due to either compositional fluctuations enhanced by phase separation in InGaN, or the strain-driven formation of ZnCdSe QDs. The conventional spectra of excitonic photoluminescence (PL) in these samples are inhomogeneously broadened, whereas employment of the techniques with high spatial resolution has allowed one to extract narrow PL lines attributed to the emission of single excitons.[31,32]

In our experiments, the PL spectra were excited by a 532-nm laser line, which is not far from the wavelength of the fundamental band edge in both structures. For the InGaN film, these conditions always imply a resonant excitation of deeply localized excitons with the localization energy in the range 100–500 meV.[10] For the CdSe/ZnSe structure, the nature of the excitation depends on the temperature. Figure 2 shows the PL spectra excited either at 532 nm (solid lines) or 325 nm (dashed lines). In the latter case the energy of the excitation is always much larger than the band-gap energy, so that the localized excitons are created nonresonantly. The shape of the emission line measured at 295 K is generally similar for both excitation wavelengths. It means that the energy of the excitons created by the 532-nm photoexcitation is above the exciton mobility edge. Certain minor deviation between the two spectra can be revealed only at the energies detuned from the laser line by the excitation energy of LO phonons.[33] At 15 K,

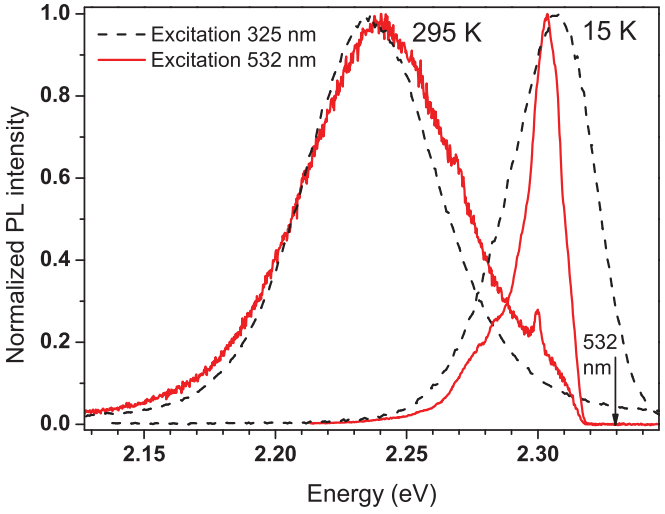

FIG. 2. (Color online) PL spectra measured in the CdSe/ZnSe structure at 295 K and 15 K with the excitation wavelength either 325 nm (dashed line) or 532 nm (solid line). The laser line at 532 nm is cut in the spectra by a notch interference filter.

the 532-nm excitation results in a noticeable narrowing of the PL line, which is a manifestation of the resonant excitation of localized excitons.

The near-field optical experiments were carried out by using a low-temperature NSOM system (Nanonics Cryo-View 2000). The illumination of the NSOM probe placed in the near field of the sample surface, as well as PL detection, were performed via a confocal optical microscope equipped with a 50× Mitutoyo objective (NA = 0.55). A noticeable PL enhancement was obtained only with apertureless probes produced by Nanonics with an attached single gold nanoparticle of 100–200 nm in diameter. More details of the experimental technique have been reported elsewhere.[10] In this paper we focus on the results, obtained with a particular probe bearing at the tip a gold particle 150 nm in diameter.

It was previously found that the effect of the tip with the attached gold particle on the shape and intensity of the PL spectrum in InGaN films strongly depends on the local morphology of the investigated surface.[10] The strongest enhancement is observed when the tip is located within a pit rather than above a protrusion of the topographical relief (see Fig. 1 in Ref. 10, demonstrating both a topographical image and a PL enhancement image measured in the same area of the $In_{0.25}Ga_{0.75}N$ sample). This was explained by the easier realization of the more efficient radial orientation of the dipole emitting light in the confocal back-scattering geometry with respect to the gold particle. Figure 3(a) shows typical μ-PL spectra of the InGaN film measured at 295 K with the excitation

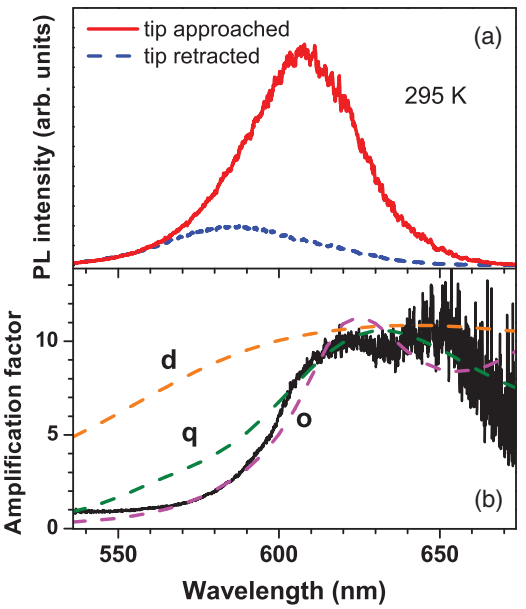

FIG. 3. (Color online) (a) Typical μ-PL spectra measured in the InGaN film at 295 K with either retracted (dashed line) or approached (solid line) NSOM probe with the attached gold particle. (b) The spectrum of the emission enhancement factor, obtained as a ratio of the two spectra presented in (a). Dashed lines show the results of a theoretical simulation performed for the "radial" orientation of the emitter for the dipole ("d," $\varepsilon_m = 1.2$, $d = 18$ nm), quadrupole ("q," $\varepsilon_m = 3.4$, $d = 15$ nm), and octupole ("o," $\varepsilon_m = 5.2$, $d = 8$ nm) resonances. The value $Y_0 = 0.001$ was chosen to fit the maximum amplification factor (∼20) measured in this sample at 295 K.

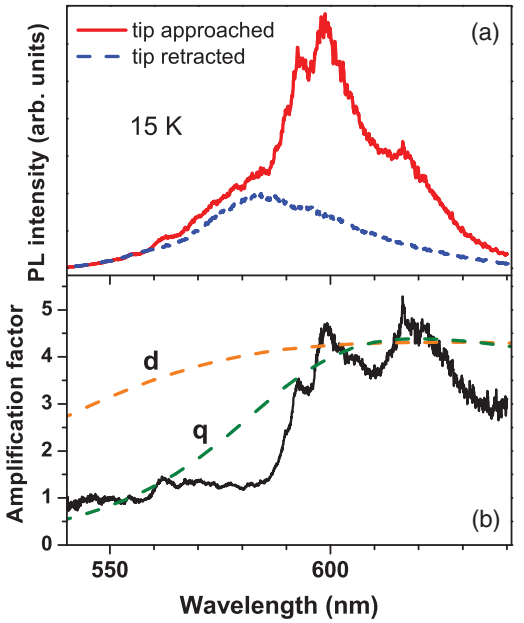

FIG. 4. (Color online) (a) Typical μ-PL spectra measured in the InGaN film at 15 K with either retracted (dashed line) or approached (solid line) NSOM probe with the attached gold particle. (b) The spectrum of the emission enhancement factor, obtained as a ratio of the two spectra presented in (a). Dashed lines show the results of a theoretical simulation performed for the radial orientation of the emitter for the dipole ("d," $\varepsilon_m = 1.0$, $d = 34$ nm) and quadrupole ("q," $\varepsilon_m = 3$, $d = 17$ nm) resonances. The value $Y_0 = 0.07$ was chosen to fit the maximum amplification factor (∼5) measured in this sample at 15 K.

laser beam focused into a spot of a diffraction-limited size with either retracted (dashed line) or approached (solid line) NSOM probe. The approached tip was located within certain pit of the rough film. Figure 3(b) demonstrates the spectrum of the emission enhancement factor, obtained as a ratio of the two spectra presented in Fig. 3(a). One can see that the maximum enhancement factor observed in the range 600–650 nm is as high as ∼10. Extensive scanning of the surface area reveals the possible range of the variation of the enhancement factor as from less than 1 up to ∼20.

Figures 4(a) and 4(b) present similar spectra measured in the InGaN film at the low temperature (15 K), when the temperature-induced broadening of the excitonic lines is negligibly small. The spectra measured with the retracted probe are generally smooth and only weakly dependent on the position at the sample surface. Contrary to that, the shape of the spectrum is extremely sensitive to the location of the approached tip. The emission line consists now of a number of superimposed peaks with different spectral widths. This behavior can be understood as the selective enhancement of a part of the inhomogeneously broadened emission spectrum by affecting only a limited number of localized excitons emitting within the near field of the gold particle.[10] The tip-induced PL enhancement observed at 15 K is weaker than at room temperature, being typically in the range 1–5 times, when the tip is located within a pit. The tip position above a protrusion usually leads to a PL quenching.

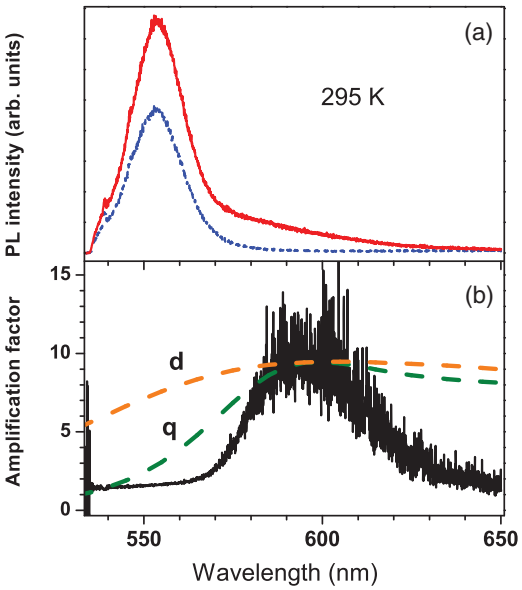

FIG. 5. (Color online) (a) Typical μ-PL spectra measured in the CdSe/ZnSe structure at 295 K with either retracted (dashed line) or approached (solid line) NSOM probe with the attached gold particle. (b) The spectrum of the emission enhancement factor, obtained as a ratio of the two spectra presented in (a). Dashed lines show the results of a theoretical simulation performed for the radial orientation of the emitter for the dipole ("d," $\varepsilon_m = 1.0$, $d = 19$ nm) and quadrupole ("q," $\varepsilon_m = 2.7$, $d = 7$ nm) resonances. The value $Y_0 = 0.007$ was chosen to fit the maximum amplification factor (~10) measured in this sample at 295 K.

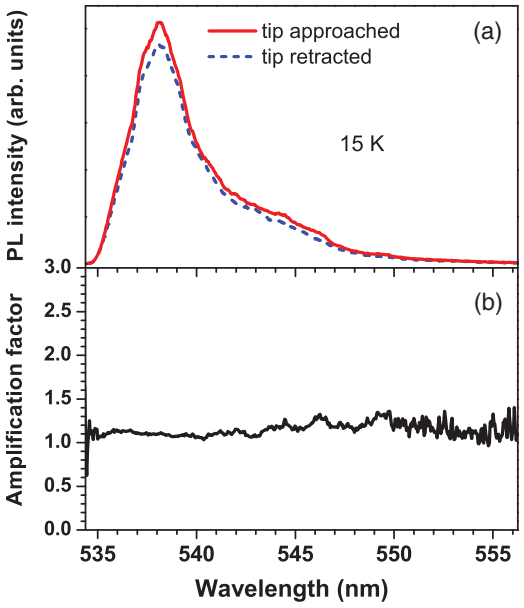

FIG. 6. (Color online) (a) Typical μ-PL spectra measured in the CdSe/ZnSe structure at 15 K with either retracted (dashed line) or approached (solid line) NSOM probe with the attached gold particle. (b) The spectrum of the emission enhancement factor, obtained as a ratio of the two spectra presented in (a).

The effect of the tip-induced enhancement in the CdSe/ZnSe QD structures is illustrated by Fig. 5 (295 K) and Fig. 6 (15 K). The emission line in this sample emerges at a shorter wavelength than in the InGaN film (~550 nm at 295 K and ~538 nm at 15 K). At 295 K the enhancement factor at the line maximum nowhere exceeds 3–4 times, while at the weak tale of the line above ~570 nm the enhancement factor can be as high as ~10 (see Fig. 5). At low temperature the enhancement factor is nearly equal to 1 in the whole spectral range at any position of the tip (see Fig. 6).

For both structures, the obtained experimental data are in general agreement with the results of the calculation, presented in Fig. 1, provided the amplification process to be governed mainly by the interaction of the excitons with the higher-order plasmon modes, excluding the dipole one. Indeed, the 150-nm gold sphere supports the dipole mode only at the wavelengths longer than ~600 nm. The emission bands observed in the InGaN film and, especially, in the CdSe/ZnSe QD structure match the very boundary of the allowed spectral range, where the effective permittivity of the semiconductor $\varepsilon_m \simeq 1$ [see Figs. 1(a) and 1(b)]. For the studied samples ε_m should be between 1 and ~7, the latter value being the permittivity of the semiconductor. The requirement $\varepsilon_m = 1$ corresponds to the gold sphere surrounded by the ambient that contradicts the experimental observation of the placement of the gold particle within a pit of the topographical relief. For the quadrupole mode, the required spectral range corresponds to ε_m between 3 and 4 [see Figs. 1(c) and 1(d)]. This implies the half-deeped gold particle in agreement with the expected configuration.

Figure 7 shows the plots of the amplification factor calculated for different wavelengths as a function of ε_m both for the radial [Fig. 7(a)] and tangential [Fig. 7(c)] orientations of the emitting dipole with respect to the surface of the 150-nm-size gold particle. The leftmost peak in the figures emerges due to the resonant interaction with the dipole mode, whereas other peaks reflect higher-order resonances. The value of the initial emission yield ($Y_0 = 0.001$) was chosen in this calculation in order to fit approximately the highest value of the amplification factor (~20) observed in the InGaN film at room temperature between 600 and 650 nm. One can see in Fig. 7(a) that for the radial orientation three resonances can provide sufficient amplification efficiency in this spectral range. The dipole resonance is active for ε_m between 1 and 2 that is the situation of the gold particle mostly surrounded by the ambient. For the radial orientation the contribution of this resonance should not be essential. Two other resonances correspond to the half-deeped particle ($3 < \varepsilon_m < 4$) and the particle deeped almost completely ($5 < \varepsilon_m < 6$). One can see in Fig. 7(b) that the decrease in the size of the gold particle makes the dipole resonance more important, whereas larger gold particles better support higher-order plasmonic modes. As expected, the tangential orientation of the emitting dipole with respect to the metal particle results in a weaker amplification or even in a reduction of the emission yield [compare Figs. 7(a) and 7(c)]. For the dipole mode the tangential amplification factor is about 20 times smaller than the radial one. One should nevertheless note that the efficiency of the plasmon-induced enhancement for the tangential geometry improves noticeably for the higher-order modes, as can be seen in Fig. 7(c).

Reasonable simulations of the amplification spectrum in the InGaN sample can be obtained for all three lowest resonances [dashed lines in Fig. 3(b)]. The calculated curves

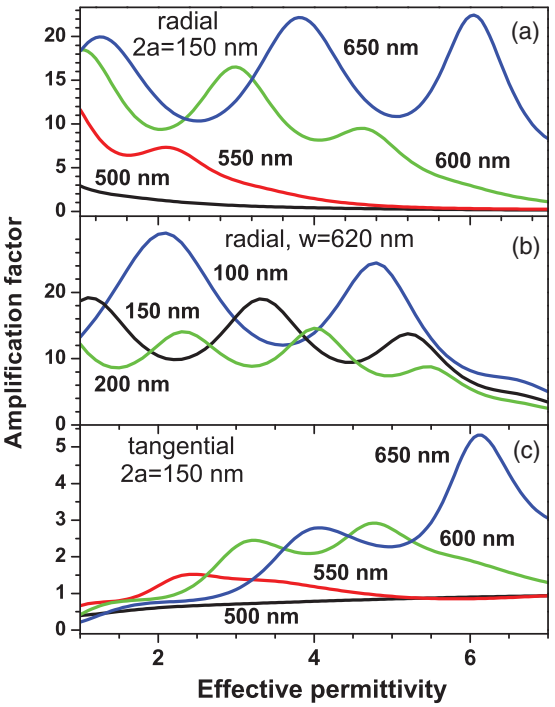

FIG. 7. (Color online) The plots of the amplification factor calculated for different wavelengths as a function of ε_m both for the radial (a) and tangential (c) orientations of the emitting dipole with respect to the surface of the 150-nm-size gold particle. (b) shows the plots calculated for the emission wavelength 620 nm for different diameters of the gold sphere (100, 150, and 200 nm). The initial emission yield of the emitter is $Y_0 = 0.001$ and the distance between the emitter and the gold sphere is 4 nm.

differ in the taken values of the effective permittivity ε_m and the emitter-particle separation. Hence each calculated spectrum reflects some particular mutual arrangement of the gold particle and the emitting dipole placed in a particular dielectric local environment. For three curves shown in Fig. 3, the choice of the parameters ensures emergence of either dipole (curve d), or quadrupole (curve q), or octupole (curve o) resonance in the spectral range 600–650 nm corresponding to the experimentally observed maximum of the amplification factor. The quality of the fit is better for the quadrupole and octupole resonances. Note also that the value of ε_m required for the fitting of the experimental data by means of the dipole resonance is unrealistically small to match the experimental conditions.

These calculations represent, in fact, an illustration rather than fitting of the experimental data. The emitting excitons can be localized at different distances from the gold particle. Furthermore, they emit light at different wavelengths, can be differently polarized, and can possess different emission yield, being localized at different places. All these parameters are not known and hence there are many ways to simulate the experimental spectrum. The distance d between the emitter and the gold particle and the initial emission yield Y_0, used in these calculations, should be considered as average values for all localized excitons emitting within the optical near field. Note that the optimum distance corresponding to the maximum amplification factor for the considered parameters is ∼4 nm.

To fit the maximum value of the amplification factor observed in the InGaN film at a low temperature (∼5), one should assume that the initial emission yield is about 0.07. The respective fits of the experimental data are shown in Fig. 4(b). Definitely, each peak in the experimental spectrum reflects the emission of an exciton or a group of excitons placed at a certain particular distance from the gold particle. The curve calculated for a single average distance provides a kind of envelope for the set of narrow lines. The optimum distance here is $d \simeq 15$ nm. Only dipole and quadrupole resonances can contribute to the light amplification for the considered set of parameters. According to these estimations, the increase in temperature from 15 to 295 K results in the 70-times decrease of the emission yield. It reasonably matches the ∼100-times reduction of the average PL intensity observed in this sample under the same conditions of excitation for the same temperature variation.

In the CdSe/ZnSe structure the emission line emerges at room temperature around 550 nm (see Fig. 5). As follows from the plots shown in Figs. 7(a) and 7(c), the amplification at this wavelength is rather inefficient. The onset of the region of strong amplification starts at about 580 nm, which is in a good agreement with the experimental findings. The fits shown in Fig. 5(b) by dashed lines are calculated for the initial emission yield $Y_0 = 0.007$. At 15 K the whole PL spectrum is below the limiting wavelength that explains the absence of any amplification (see Fig. 6). The average PL intensity in this sample increases by ∼75 times with the temperature variation from 295 to 15 K. Then, multiplying the value $Y_0 = 0.007$ by 75, one can estimate the low-temperature emission yield in this sample as 52%. The relatively small emission yield can be explained by the fact that noticeable amplification in this sample is observed in the places, where the flatness of the surface is disturbed due to the emergence of extended defects that can be responsible for enhanced nonradiative recombination.

Finally, we comment on the limitations of the used electrodynamic approach as applied for interpretation of the experimental data on site-selective amplification of light in semiconductor heterostructures. The first important approximation concerns the validity of the applied model of the metal sphere for the description of the properties of the used NSOM probes. Any deviation of the shape of the attached particle from the spherical one can result in a variation of the position and intensity of the plasmon resonances. Moreover, the attachment of the particle to the tip changes its dielectric environment and hence effects the plasmonic properties. Currently, the nanoscale control over the properties of the probes of this type is not quite sufficient. The action of the particular probe selected for the experiments described in this paper can be consistently explained in terms of the applied simple electrodynamic model. However, the dispersion of the properties between different available probes is essential and the development of the reliable fabrication technique has been yet a challenge.

Another simplification concerns ignoring of the plasmon-induced local increase of the exciting electromagnetic field in the vicinity of the metal particle. In fact, this is the counterpart of the Purcell effect, which also follows from the local increase in the density of the photonic modes (see, e.g., Ref. 18). In our experiments, we can exclude this

factor by several reasons. First of all, the 150-nm-size gold particle does not support any distinctive plasmon resonance at the excitation wavelength 532 nm. Therefore the respective electromagnetic enhancement factor should be small. Besides, one can expect that the main body of the probe partly prevents direct lighting of the particle attached to the tip from below. Under these conditions, the excitons can be excited quite far from the tip and approach its near-field region due to some transport mechanism. Note that the spatial dynamics of excitons is completely neglected in the presented analysis. This is justified for the condition of strong amplification, when the enhanced emission rate can be much faster than the rate of the hopping dynamics. On the other hand, for the weak and moderate amplifications the emission and escape lifetimes can be comparable and then the dynamical factor might be important. Note also that the experimental amplification factor, obtained as the ratio of the emission intensities measured for the approached and retracted probe, is always underestimated due to the emission from the area of the excitation spot outside the near field of the gold particle. This deviation is more pronounced for weaker amplification factors.

IV. CONCLUSIONS

We demonstrate that under certain conditions the plasmon-induced enhancement of the emission can be a useful phenomenon allowing noticeable improvements of the radiative properties of individual localized excitons in epitaxial semiconductor heterostructures. The enhancement of the excitonic emission due to the interaction with plasmons in a gold particle was observed experimentally in an $In_{0.25}Ga_{0.75}N$ film and a CdSe/ZnSe QD heterostructure grown by MBE. The experimental results are explained in the framework of an exact electrodynamic theory making allowance for the interaction with higher-order plasmon modes in a spherical metal particle. In particular, for the $In_{0.25}Ga_{0.75}N$ film with the room-temperature emission yield as low as ∼0.1% the proper use of the plasmonic enhancement allows one to increase the emission yield up to ∼2%. It is shown that this enhancement owes mainly to the resonant interaction of the localized excitons with the quadrupole and octupole plasmon modes in the gold particle. One should note that the conclusion about the dominant role of the higher-order resonances in the considered spectral range is valid for the gold particles with the diameter exceeding ∼100 nm [see Fig. 7(b)].

The device implementation of this scheme can, nevertheless, be intricate since the metal-semiconductor structures should comply with many strict requirements, including the fulfillment of the resonance between the frequencies of the emitting dipoles and the plasmon and of the polarization selection rules, realization of high enough values of the field enhancement factors, and accurate engineering of the balance between the radiation and dissipation in the metal structures. Most efficient amplification by means of the gold nanoparticle can be obtained for the semiconductor structures emitting in the range 700–900 nm, where the imaginary part of the dielectric function of gold is minimal. For the optimized conditions the maximum possible value of the light amplification factor K_{em} is as high as ∼140 for the initial emission yield $Y_0 = 0.001$ and yet noticeable (∼5) for $Y_0 = 0.1$. These data allow one to consider the mechanism of plasmon-induced light enhancement as a promising tool for engineering semiconductor single-photon sources operating at room temperature.

ACKNOWLEDGMENTS

This work has been supported in part by the RFBR (Grant Nos. 09-02-01305a, 10-02-00633a, and 11-02-12220-ofi-m), project FP7 ITN SPIN-OPTRONICS, and the Program of the Presidium of RAS.

[1] E. M. Purcell, Phys. Rev. **69**, 681 (1946).
[2] R. M. Amos and W. L. Barnes, Phys. Rev. B **55**, 7249 (1997).
[3] J. R. Lakowicz, Anal. Biochem. **298**, 1 (2001).
[4] J. N. Farahani, D. W. Pohl, H.-J. Eisler, and B. Hecht, Phys. Rev. Lett. **95**, 017402 (2005).
[5] Y. Ito, K. Matsuda, and Y. Kanemitsu, Phys. Rev. B **75**, 033309 (2007).
[6] A. V. Akimov, A. Mukherjee, C. L. Yu, D. E. Chang, A. S. Zibrov, P. R. Hemmer, H. Park, and M. D. Lukin, Nature (London) **450**, 402 (2007).
[7] C. T. Yuan, P. Yu, and J. Tang, Appl. Phys. Lett. **94**, 243108 (2009).
[8] S. Masuo, H. Naiki, S. Machida, and A. Itaya, Appl. Phys. Lett. **95**, 193106 (2009).
[9] X.-W. Wu, M. Gong, C.-H. Dong, J.-M. Cui, Y. Yang, F.-W. Sun, G.-C. Guo, and Z.-F. Han, Opt. Express **18**, 6340 (2010).
[10] A. A. Toropov, T. V. Shubina, V. N. Jmerik, S. V. Ivanov, Y. Ogawa, and F. Minami, Phys. Rev. Lett. **103**, 037403 (2009).
[11] A. Urbańczyk, G. J. Hamhuis, and R. Nötzel, Appl. Phys. Lett. **97**, 043105 (2010).
[12] P. Michler, A. Kiraz, C. Becher, W. V. Schoenfeld, P. M. Petroff, L. Zhang, E. Hu, and A. Imamoğlu, Science **290**, 2282 (2000).
[13] C. Santori, D. Fattal, J. Vučković, G. S. Solomon, and Y. Yamamoto, Nature (London) **419**, 594 (2002).
[14] H. Mertens, A. F. Koenderink, and A. Polman, Phys. Rev. B **76**, 115123 (2007).
[15] D. Bimberg, M. Grundmann, and N. N. Ledentsov, *Quantum Dot Heterostructures* (John Wiley & Sons, Chichester, 1999).
[16] J. Gersten and A. Nitzan, J. Chem. Phys. **75**, 1139 (1981).
[17] D. A. Weitz, S. Garoff, J. Gersten, and A. Nitzan, J. Chem. Phys. **78**, 5324 (1983).
[18] W. L. Barnes, J. Mod. Opt. **45**, 661 (1998).
[19] A. O. Govorov, G. W. Bryant, W. Zhang, T. Skeini, J. Lee, N. A. Kotov, J. M. Slocik, and R. R. Naik, Nano Lett. **6**, 984 (2006).
[20] H. Kuwata, H. Tamaru, K. Esumi, and K. Miyano, Appl. Phys. Lett. **83**, 4625 (2003).
[21] B. van der Pol and H. Bremmer, Philos. Mag. Ser. 7 **24**, 141 (1937).
[22] V. A. Fock, *Electromagnetic Diffraction and Propagation Problems* (Pergamon, New York, 1965).
[23] R. Rupin, J. Chem. Phys. **76**, 1681 (1982).

[24]Y. S. Kim, P. T. Leung, and T. F. George, Surf. Sci. **195**, 1 (1988).
[25]P. B. Johnson and R. W. Christy, Phys. Rev. B **6**, 4370 (1972).
[26]A. Polimeni, A. Patanè, M. Henini, L. Eaves, and P. C. Main, Phys. Rev. B **59**, 5064 (1999).
[27]R. Leon, S. Fafard, D. Leonard, J. L. Merz, and P. M. Petroff, Appl. Phys. Lett. **67**, 521 (1995).
[28]V. N. Jmerik, A. M. Mizerov, T. V. Shubina, M. Yagovkina, V. B. Listoshin, A. A. Sitnikova, S. V. Ivanov, M.-H. Kim, M. Koike, and B.-J. Kim, J. Cryst. Growth **301–302**, 469 (2007).
[29]A. A. Toropov, S. V. Ivanov, T. V. Shubina, S. V. Sorokin, A. V. Lebedev, A. A. Sitnikova, P. S. Kop'ev, M. Willander, G. Pozina, P. Bergman, and B. Monemar, Jpn. J. Appl. Phys. **38**, 566 (1999).
[30]T. V. Shubina, A. A. Sitnikova, V. A. Solov'ev, A. A. Toropov, I. V. Sedova, S. V. Ivanov, M. Keim, A. Waag, and G. Landwehr, J. Cryst. Growth **214-215**, 727 (2000).
[31]J. H. Rice, J. W. Robinson, A. Jarjour, R. A. Taylor, R. A. Oliver, G. A. D. Briggs, M. J. Kappers, and C. J. Humphreys Appl. Phys. Lett. **84**, 4110 (2004).
[32]B. Patton, W. Langbein, and U. Woggon, Phys. Rev. B **68**, 125316 (2003).
[33]A. A. Toropov, T. V. Shubina, S. V. Sorokin, A. V. Lebedev, R. N. Kyutt, S. V. Ivanov, M. Karlsteen, M. Willander, G. R. Pozina, J. P. Bergman, and B. Monemar, Phys. Rev. B **59**, R2510 (1999).